京都大学
KYOTO UNIVERSITY

Title	Transport of ballistic projectiles during the 2015 Aso Strombolian eruptions
Author(s)	Tsunematsu, Kae; Ishii, Kyoka; Yokoo, Akihiko
Citation	Earth, Planets and Space (2019), 71
Issue Date	2019-04-27
URL	http://hdl.handle.net/2433/241797
Right	© The Author(s) 2019. This article is distributed under the terms of the Creative Commons Attribution 4.0 International License (http://creativecommons.org/licenses/by/4.0/), which permits unrestricted use, distribution, and reproduction in any medium, provided you give appropriate credit to the original author(s) and the source, provide a link to the Creative Commons license, and indicate if changes were made.
Type	Journal Article
Textversion	publisher

FULL PAPER

Open Access

Transport of ballistic projectiles during the 2015 Aso Strombolian eruptions

Kae Tsunematsu[1,2]* , Kyoka Ishii[3,4] and Akihiko Yokoo[4]

Abstract

Large pyroclasts—often called ballistic projectiles—cause many casualties and serious damage on people and infrastructures. One useful measure of avoiding such disasters is to numerically simulate the ballistic trajectories and forecast where large pyroclasts deposit. Numerical models are based on the transport dynamics of these particles. Therefore, in order to accurately forecast the spatial distribution of these particles, large pyroclasts from the 2015 Aso Strombolian eruptions were observed with a video camera. In order to extrapolate the mechanism of particle transport, we have analyzed the frame-by-frame images and obtained particle trajectories. Using the trajectory data, we investigated the features of Strombolian activity such as ejection velocity, explosion energy, and particle release depth. As gas flow around airborne particles can be one of the strongest controlling factors of particle transport, the gas flow velocities were estimated by comparing the simulated and observed trajectories. The range of the ejection velocity of the observed eruptions was 5.1–35.5 m/s, while the gas flow velocity, which is larger than the ejection velocity, reached a maximum of 90 m/s, with mean values of 25–52 m/s for each bursting event. The particle release depth, where pyroclasts start to move separately from the chunk of magmatic fragments, was estimated to be 11–13 m using linear extrapolation of the trajectories. Although these parabolic trajectories provide us with an illusion of particles unaffected by the gas flow, the parameter values show that the particles are transported by the gas flow, which is possibly released from inside the conduit.

Keywords: Ballistics, Gas flow, Image analysis, Acoustic energy, Strombolian eruptions

Introduction

Large pyroclasts (> 10 cm in diameter), often called ballistic projectiles, are ballistic blocks or bombs. They are defined as particles which draw a parabolic trajectory in the air and deposit around the vent. They are not included in the gas–pyroclasts mixture or normally fly out from the volcanic plume. The pyroclasts are hazardous, and sometimes kill people with their destructive energy. Casualties have been reported from volcanoes all over the world: Galeras, Yasur, Popocatepetle, Pacaya (Baxter and Gresham 1997; Cole et al. 2006; Alatorre-Ibargüengoitia et al. 2012; Wardman et al. 2012). Recently, more than 50 people were killed by the 2014 Mt. Ontake eruption and most of the fatalities were caused by ballistic projectiles

(Oikawa et al. 2016; Tsunematsu et al. 2016; Yamaoka et al. 2016). Another fatality occurred at Mt. Kusatsu in January 2018 (Mainichi Shimbun 2018) despite the growing awareness (among the public) of the dangers posed by ballistic projectiles, following the Ontake eruption. It is hard to forecast the starting time of phreatic eruptions (Stix and Maarten de Moor 2018). Therefore, in order to avoid such disasters, one should produce hazard maps showing the likely impact area of ballistic projectiles and provide useful guidelines for delineating evacuation zones. Here, we use a numerical simulation based on the dynamics of pyroclast transport to provide constraints on a specific eruption—the 2015 Aso eruptions. We used this as a case study for comparing modeled data with observed particle trajectories. Even though the fatal eruptions reported in the literature were mostly phreatic eruptions, we observed magmatic Strombolian eruptions, because it is difficult to forecast when and where phreatic eruptions will occur. In contrast to the

*Correspondence: kae_tsunematsu@sci.kj.yamagata-u.ac.jp
[1] Faculty of Science, Yamagata University, Yamagata-shi 990-8560, Yamagata, Japan
Full list of author information is available at the end of the article

Tsunematsu *et al. Earth, Planets and Space*   (2019) 71:49

Page 2 of 14

phreatic eruptions, Strombolian eruptions of the Aso volcano occurred intermittently with intervals of minutes to hours. In this study, we provide a unique dataset with which to explore the governing dynamics of ballistic ejecta and discuss its wide applicability for other ballistic studies globally.

The dynamics of ballistic transport in volcanic eruptions are studied using the field observation of deposits (Biass et al. 2016; Fitzgerald et al. 2014; Kilgour et al. 2010; Pistolesi et al. 2011; Swanson et al. 2012; Houghton et al. 2017), by video analysis (Chouet et al. 1974; Iguchi and Kamo 1984; Patrick et al. 2007; Gaudin et al. 2014; Taddeucci et al. 2012, 2014, 2015), by laboratory or field experiments (Alatorre-Ibargüengoitia and DelgadoGranados 2006; Alatorre-Ibargüengoitia et al. 2010; Graettinger et al. 2014, 2015) and by numerical simulations (de' Michieli Vitturi et al. 2010; Tsunematsu et al. 2014, 2016; Alatorre-Ibargüengoitia et al. 2016; Biass et al. 2016). However, there are still some unanswered questions. One of the most important questions is how the gas flow around particles affects the transport dynamics.

Several numerical models of ballistics and large pyroclasts were based on the particle velocity with the drag due to the static atmosphere. The model of Mastin (2001) calculated the drag including a "reduced drag zone", which is defined as a zone where the drag is negligible or absent. The idea of this zone was suggested by reference to Fagents and Wilson (1993), who advocated the model of the velocity decay near the vent in a Vulcanian eruption due to the confined gas pressure under the caprock. It means that the "reduced drag zone" is the zone where the air drag is apparently reduced due to the gas flow. The gas flow around particles mainly consists of the volcanic gas in the eruptive mixture and the atmosphere (Taddeucci et al. 2015). de' Michieli Vitturi et al. (2010) also proposed a model for large pyroclast transport coupling particles and gas flow. Therefore, it is better to obtain the gas flow velocity directly from the observation and apply it to the numerical simulation for assessing the impacted area by ballistic projectiles.

Not so many observations of gas flow velocity have been reported in the literature (Gouhier and Donnadieu 2010, 2011). During Vulcanian eruptions, we need to be at a safe distance, but still close enough to shoot the film at a sufficiently high resolution to recognize large pyroclasts. Therefore, we observed Strombolian eruptions which occurred intermittently with intervals of minutes to hours, and deduced the gas flow velocity from the video images of large pyroclasts.

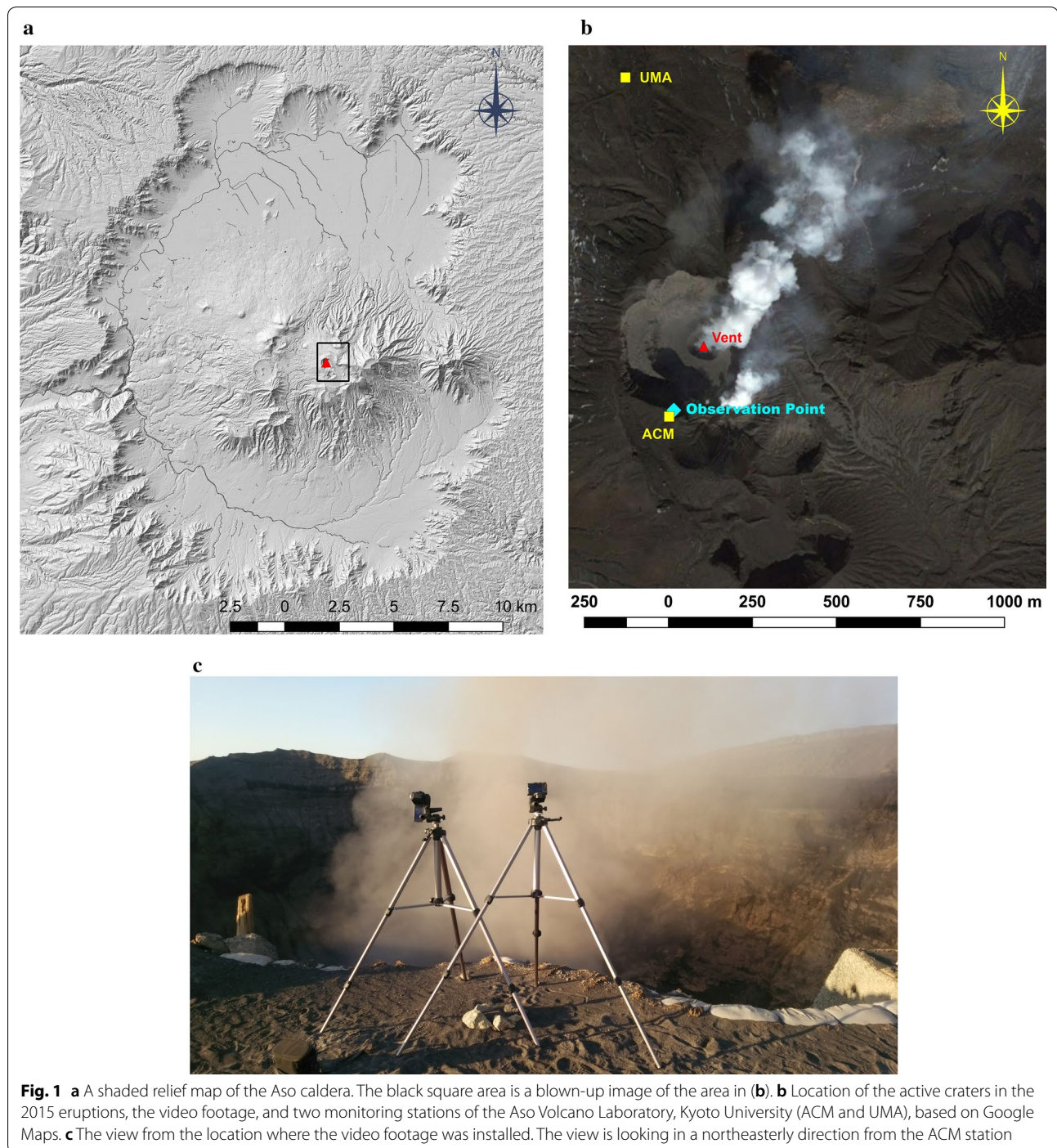Our idea is to estimate the flow velocity by comparing the simulated and observed trajectories by varying the drag coefficient. The momentum equation of ballistic transport widely used (Alatorre-Ibargüengoitia et al. 2016; Fitzgerald et al. 2014; Tsunematsu et al. 2016) is as follows.

$$m\frac{D\vec{v}}{Dt} = -\frac{AC_D\rho_a(\vec{v} - \vec{u})|\vec{v} - \vec{u}|}{2} - m\vec{g}, \qquad (1)$$

where m is the mass of a ballistic block (particle), A is the cross-sectional area of the particle perpendicular to the flow direction, C_D is the drag coefficient, ρ_a is the air density, g is the acceleration due to gravity, $\boldsymbol{v}$ is the particle velocity, and $\boldsymbol{u}$ is the velocity of gas flow. The drag term is the first term on the right-hand side. As is shown in the drag term, parameters such as C_D, A, and the density of particle ρ_p, which is linked with the mass as $m = \frac{\pi D^3}{6}\rho_p$ (where D is the particle diameter and ρ_p is the particle density) assuming that particles are spherical, are constitutive parameters. The difference between the particle velocity and the gas flow velocity is a strong factor because it is squared in the drag term. Simulations of large pyroclast transport assigning (or substituting) the realistic gas flow velocity into the model equation would make it possible to forecast the realistic travel distances of large pyroclasts.

Strombolian eruptions were well studied in the Stromboli volcano (Ripepe et al. 1993; Patrick et al. 2007; Pistolesi et al. 2011; Taddeucci et al. 2012, 2014, 2015; Bombrun et al. 2015; Gaudin et al. 2014; Capponi et al. 2016). Strombolian eruptions have been observed in only a few other volcanoes, for example, Mt. Erebus (Aster et al. 2003; Johnson and Aster 2005; Dibble et al. 2008), Yasur Volcano (Meier et al. 2016; Spina et al. 2015), Heimaey (Self et al. 1974; Blackburn et al. 1976), Etna (McGetchin et al. 1974; Gouhier and Donnadieu 2010, 2011) and Alaid (Steinberg and Babenko 1978). Activities of Strombolian eruptions do not always have the same characteristics (e.g., ejection velocity, energy). Therefore, it is worth observing different volcanoes, especially if the volcanic vent area is accessible during the eruption—like it was during the Strombolian activity around the first crater of Aso Nakadake.

Aso volcano is located at the center of Kyushu Island in southwest Japan and is one of the most active volcanoes in the country. Four gigantic pyroclastic flow activities occurred from 300 to 70 ka, which are called Aso-1- Aso-4 eruptions (Ono and Watanabe 1985). The Aso-4 eruption formed the current Aso caldera (Fig. 1a), and after the eruption the Aso bulk composition changed from a basaltic to rhyolitic composition. Inside this caldera, there are 17 cones but only the Nakadake central cone is currently active. In the last 80 years, the Nakadake activity has included ash emissions, incandescence and Strombolian activity emitting basaltic andesite to andesite magma. The 2014–2015

Tsunematsu *et al. Earth, Planets and Space* (2019) 71:49

Page 3 of 14

Fig. 1 a A shaded relief map of the Aso caldera. The black square area is a blown-up image of the area in (**b**). **b** Location of the active craters in the 2015 eruptions, the video footage, and two monitoring stations of the Aso Volcano Laboratory, Kyoto University (ACM and UMA), based on Google Maps. **c** The view from the location where the video footage was installed. The view is looking in a northeasterly direction from the ACM station

eruption episode included a mixture of these three phenomena and the magma showed an andesitic composition (Saito et al. 2018). Intermittent eruption activity started in November 2014 at the Nakadake first crater (Fig. 1b). Eruptive activities reached their climax from

the end of January to the beginning of February 2015 (Zobin and Sudo 2017), and Strombolian and ash-emission activities continued intermittently until the end of April 2015 (Yokoo and Miyabuchi 2015). We carried out a video observation on April 25, 2015.

Tsunematsu *et al. Earth, Planets and Space*   (2019) 71:49

Page 4 of 14
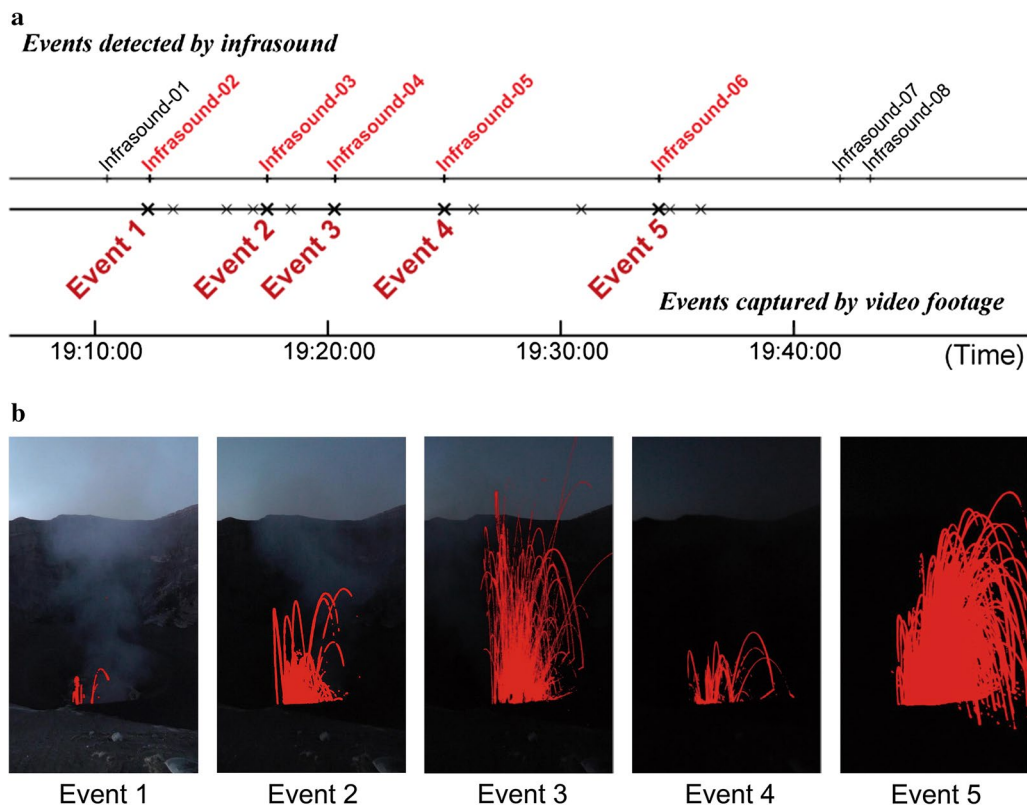
Fig. 2 a Time sequence and events detected via infrasound and video footage. The upper line shows the events detected by infrasound, and the lower line shows events detected by the camera. Red characters show the events detected by both infrasound and video footage. **b** Synchronized frame images during each bursting event

## Method

Setup of the monitoring facilities

The Strombolian eruption was observed from the edge of the cliff, approximately 200 m from the vent center, looking down on the crater with a declination angle of 28° (Fig. 1b). One video camera (Panasonic HV-C700: frame rate was 29.97 frames per second) and an automatic digital camera were installed at the observation point shown in Fig. 1(b, c). The monitoring was carried out from around 3 pm to 8 pm at Japan Standard Time (JST) on April 25, 2015. 21 bursting events were observed, but some particles were not discernable within the video image because of the strong daylight. Only the events that occurred after 7 pm were observed with good contrast between the darkness and the particles (Fig. 2).

To compare the energy of events, based on the acoustic and seismic signals, it is necessary to utilize events detected by both acoustic and video equipment. Therefore, we selected five events which had both acoustic and video data between 7 and 8 pm (Fig. 2a).

Image analysis

The obtained video images were cut out into frames, and the resolution of each frame image was 1920×1080 pixels. Given that the video footage was taken from the edge of a depression larger than the eruption vent, the images were calibrated taking into consideration the camera lens distortion. The camera lens distortion is corrected by the camera characteristics of the Panasonic HV-C700. We assumed that our focused screen was above the eruptive vent and tilted because of the declination of the camera, with the latter calculated from the aspect ratio of the vent captured on the video image assuming that the real vent shape is circular. In fact, the vent shape was circular from a bird's-eye view (Fig. 1b). We transformed all images using the rotation matrix with the tilt angle (28°). The relationship between pixel value and the actual length was calculated using a digital elevation model (DEM) and the obtained images. The DEM was constructed using the UAV observation of Yokoo et al. (2019). Consequently, the horizontal resolution was 5.81 cm/pixel and the vertical resolution was 3.95 cm/pixel.

A conceptual flowchart of whole image analyses is shown in Fig. 3. Video images were cut into frames

Tsunematsu *et al. Earth, Planets and Space*   (2019) 71:49

Page 5 of 14
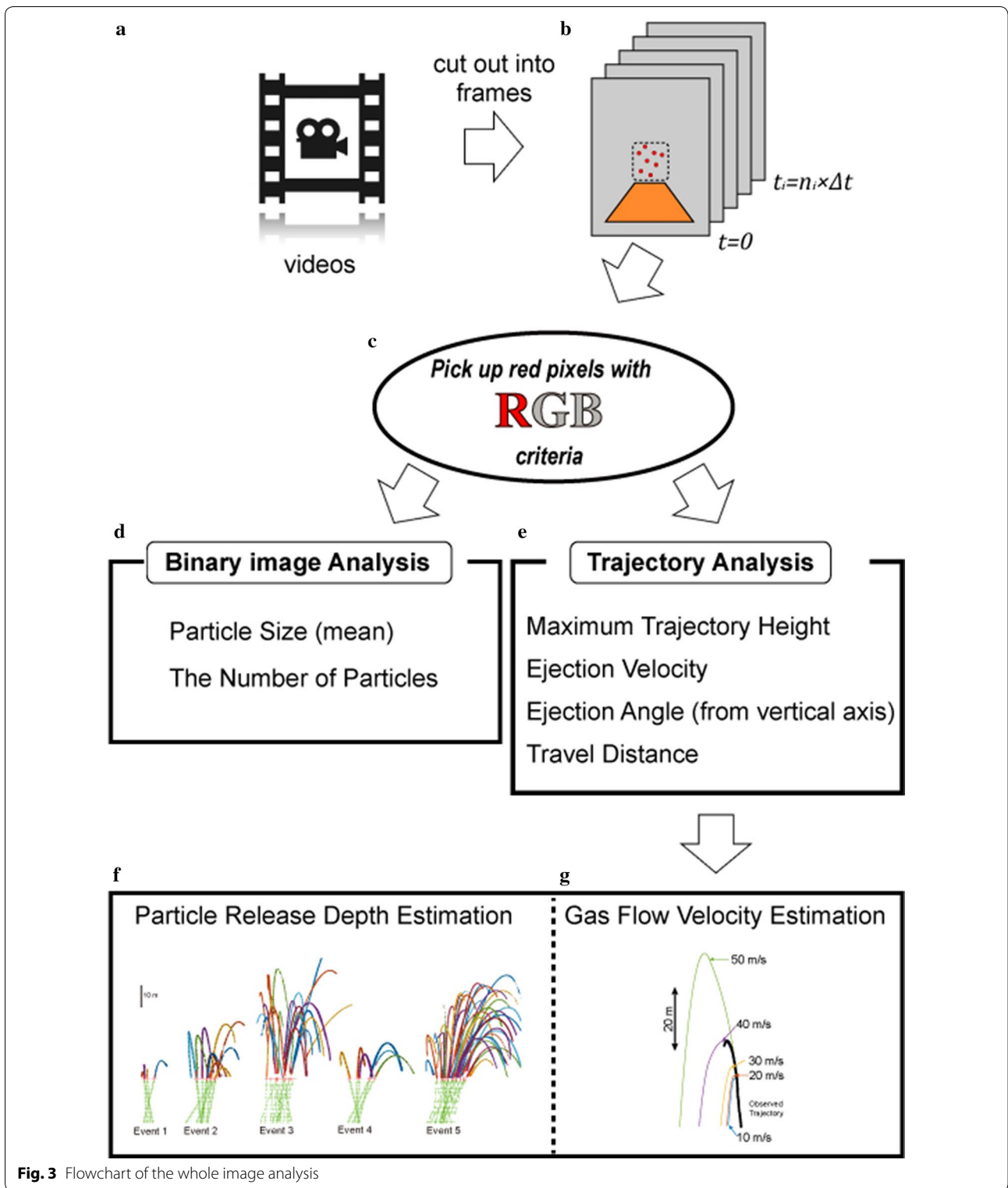
Fig. 3 Flowchart of the whole image analysis

(Fig. 3a, b). After cutting images from the video, the red-glowing pixels in each frame image were recognized using the RGB criteria (where R, G and B denote the value of color in the RGB color model) which we had defined by trying several criteria (Fig. 3c). The details

Tsunematsu *et al. Earth, Planets and Space* (2019) 71:49

Page 6 of 14

Table 1 Characteristic parameters of each event obtained from binary images (*1) and trajectory analysis (*2)

| Parameter	Event 1 (4)	Event 2 (10)	Event 3 (23)	Event 4 (6)	Event 5 (39)
Mean particle size in a frame (m)*1	0.19	0.19	0.22	0.26	0.25
Approximate particle number in a frame*1	1.2	11.7	61.1	16.7	176.9
Maximum of all trajectory heights (m)*2	7.7	25.6	57.7	15.7	44.0
Mean ± standard deviation of ejection velocity (m)*2	6.0 ± 1.0	10.9 ± 2.4	18.8 ± 5.3	9.6 ± 0.7	15.5 ± 3.9
Mean ± standard deviation of ejection angle from vertical axis (°)*2	4.6 ± 2.9	7.1 ± 4.7	6.4 ± 4.2	10.8 ± 6.9	11.1 ± 6.6
Maximum travel distance (m)	8.9	11.9	17.8	13.8	17.8

The numbers under each event name in parentheses are the number of trajectories which could be extracted for each event

defining each criterion are explained in the Additional file 1 (A).

The following image analyses consist of the binarization analysis (Fig. 3d) and trajectory analysis (Fig. 3e). The binarization analysis has been implemented using each frame image to extract the information of particle size and the number of particles. The particles were turned into white and the background area was turned into black in each frame. Consequently, the mean particle size and the approximate particle number are obtained for each event. The details of the binarization process are also explained in the Additional file 1 (B).

The trajectory analysis is performed for 4, 10, 23, 6 and 39 trajectories (82 in total) for events 1–5, respectively (Table 1). The two-dimensional trajectories of particles are derived by merging all frames over the event period. The details of the trajectory analysis are explained in the Additional file 1 (C). Using the extracted trajectories from the video footage, we defined the maximum trajectory height which particles reached, the ejection velocity, the ejection angle and the travel distance (Fig. 3e). Using the trajectory data, we estimated the particle release depth (Fig. 3f) and the gas flow velocity (Fig. 3g). The particle release depth estimation is explained in the discussion section. The method for the estimation of the flow velocity is explained in the next "Estimation of the flow velocity" section.

The ejection velocity was calculated using the time–velocity relationship as shown in Fig. 4. Unfortunately, we did not measure the velocity component toward or away from the camera because we only used one video camera. Mostly, the plots of (t, v_x) and (t, v_y) appear as straight lines on the graph and these plots were fit with linear equations, where t denotes time, v_x denotes the velocity on the horizontal axis, and v_y denotes the velocity on the vertical axis. We assumed that the vertical and horizontal velocities decrease at a constant rate. To obtain the ejection velocity, the velocity lines in the vertical direction were fit with a linear equation and extrapolated until the
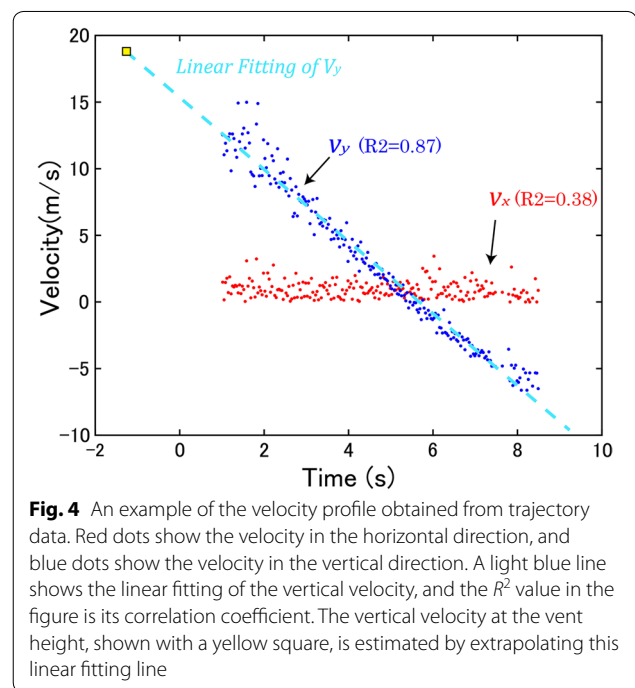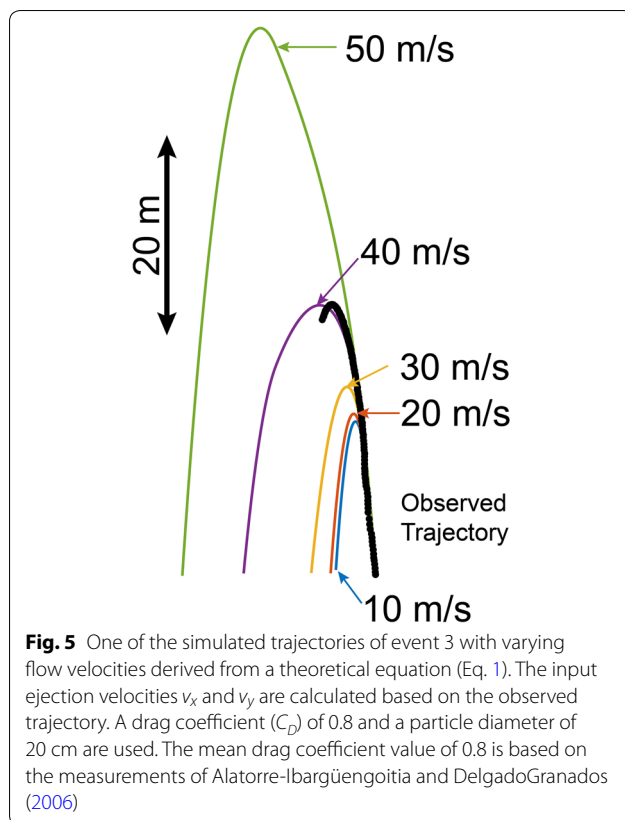

Fig. 4 An example of the velocity profile obtained from trajectory data. Red dots show the velocity in the horizontal direction, and blue dots show the velocity in the vertical direction. A light blue line shows the linear fitting of the vertical velocity, and the R^2 value in the figure is its correlation coefficient. The vertical velocity at the vent height, shown with a yellow square, is estimated by extrapolating this linear fitting line

ejection height (Fig. 4). The ejection angle θ was defined with the velocity component v_x and v_y as $\theta = 90 - \gamma$, where $\tan \gamma = \frac{v_y}{v_x}$. The maximum height of each trajectory was read from the trajectory in the vertical direction. The travel distance was measured as the horizontal width of each trajectory. These values of travel distance were underestimated because we did not have the velocity component away from the camera.

Estimation of the flow velocity

We used Eq. (1) to simulate trajectories with a variable gas flow velocity $\boldsymbol{u}$ of 10–100 m/s. Input parameters were ejection velocity, particle density, particle diameter and the drag coefficient. The values of ejection velocities v_x and v_y and particle size were obtained by

Tsunematsu *et al. Earth, Planets and Space* (2019) 71:49

Page 7 of 14

Fig. 5 One of the simulated trajectories of event 3 with varying flow velocities derived from a theoretical equation (Eq. 1). The input ejection velocities v_x and v_y are calculated based on the observed trajectory. A drag coefficient (C_D) of 0.8 and a particle diameter of 20 cm are used. The mean drag coefficient value of 0.8 is based on the measurements of Alatorre-Ibargüengoitia and DelgadoGranados (2006)

trajectory analysis. The particle density was measured using the method of Shea et al. (2010) by measuring the wet and dry weight of particles. It was impossible to take samples on the day of the observation because the eruption continued during and after the observation, while three clasts were sampled on April 29, 4 days after our observation. One of these samples was used for the density measurement. The obtained density value was 616.7 kg/m³. The drag coefficient was varied from 0.6 to 1.2 with reference to the measurement of Alatorre-Ibargüengoitia and DelgadoGranados (2006).

The gas flow velocity was calculated in the same direction as the ejection velocity for each trajectory simulation. An example of the comparison is shown in Fig. 5. In this example, the observed trajectory is as high as the simulated trajectory with a gas flow velocity of 40 m/s. Thus, we estimated the gas flow velocity to be 40 m/s. If the observed trajectory is shown in between the simulated trajectories with a gas flow velocity ranging from 30 to 40 m/s, we estimated the gas flow velocity as 35 m/s. Therefore, for this estimation, the gas flow velocity has a resolution of 5 m/s.

Results

Characteristic parameters obtained from trajectories and particle images

In order to reveal the characteristic features of the 2015 Aso Strombolian eruptions, the mean particle size, the approximate particle number, the maximum trajectory height, the mean ejection velocity and the mean ejection angle for each burst event were derived from the image analysis as shown in Table 1.

The mean particle size measured from the cut-out image for each time frame of the video was in the range of 19–26 cm (Table 1).

The particle size and total number of particles were also obtained from black-and-white images. Particle number is an approximate value because one frame was selected from many frames, but airborne particles that were in one frame may no longer be airborne in subsequent frames. Therefore, the number of particles is an underestimate of the total number of particles in an event.

The maximum trajectory heights, the mean ejection velocities and the mean ejection angles were calculated for each particle trajectory extracted from each event record. During the trajectory analysis, we were not able to extract all of the trajectories because some of them were quite close to each other, especially where particles are concentrated around the crater. Most of the particle trajectories were in our video frame, while only one trajectory from event 3 went higher than our frame boundary. Even though the highest maximum trajectory occurred in event 3, the real maximum was higher than the largest recorded value, and so it must have been more than 60 m above the vent rim. The mean ejection velocity was calculated for each event from the velocity profile. The maximum value (18.8 m/s) of the mean ejection velocity was estimated for event 3, and the minimum value (6.0 m/s) for event 1 (Table 1). Among all trajectories, the maximum value was 35.5 m/s (the highest trajectory of event 3) and the minimum value was 5.1 m/s (the lowest trajectory of event 1). The range of ejection angles was 0.1°–25.8°, while the range of mean ejection angles was 4.6°–11.1° (Table 1). The range of travel distances was 8.9–17.8 m (Table 1).

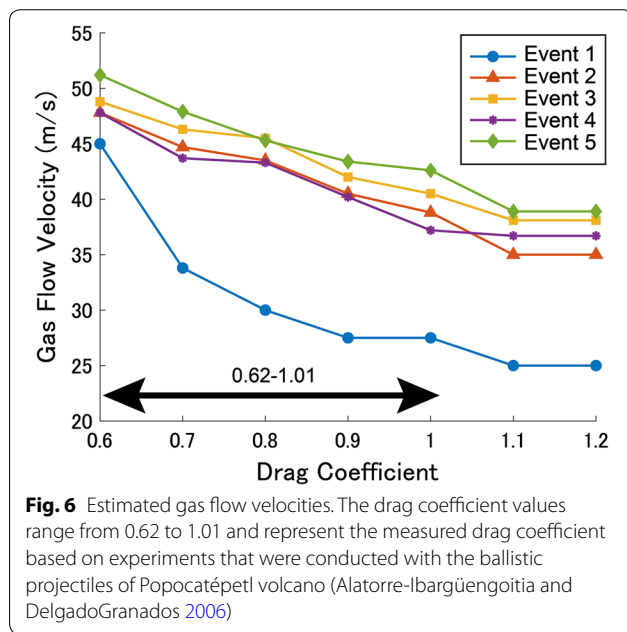### Estimation of the flow velocity

By comparing the observed and simulated trajectories, we estimated the gas flow velocity. The mean flow velocity for each event with the standard deviation is shown in Table 2 and the mean values are plotted in Fig. 6. The estimated gas flow velocity for each event decreases as the drag coefficient value increases. The fastest flow velocity is estimated to be 90 m/s for the maximum trajectory of event 3 with the drag coefficient $C_D = 0.6$.

Table 2 Estimated gas flow velocities (m/s) derived by comparing simulated and observed trajectories

	Cd = 0.6	Cd = 0.7	Cd = 0.8	Cd = 0.9	Cd = 1.0	Cd = 1.1	Cd = 1.2
Event 1	45.0 ± 0.0	33.8 ± 8.5	30.0 ± 10.0	27.5 ± 5.0	27.5 ± 5.0	25.0 ± 0.0	25.0 ± 0.0
Event 2	47.8 ± 4.2	44.7 ± 4.8	43.5 ± 3.4	40.5 ± 5.0	38.8 ± 3.7	35.0 ± 4.7	35.0 ± 4.7
Event 3	48.8 ± 16.7	46.3 ± 14.8	45.5 ± 14.0	42.0 ± 13.6	40.5 ± 12.9	38.1 ± 11.7	38.1 ± 11.7
Event 4	47.8 ± 7.8	43.7 ± 9.1	43.3 ± 9.8	40.2 ± 7.9	37.2 ± 7.2	36.7 ± 7.5	36.7 ± 7.5
Event 5	51.2 ± 10.8	47.9 ± 10.5	45.3 ± 9.4	43.4 ± 8.6	42.6 ± 8.1	38.9 ± 7.6	38.9 ± 7.6

The values are shown as "mean ± standard deviation" in each cell. Mean values are also shown in Fig. 6

Fig. 6 Estimated gas flow velocities. The drag coefficient values range from 0.62 to 1.01 and represent the measured drag coefficient based on experiments that were conducted with the ballistic projectiles of Popocatépetl volcano (Alatorre-Ibargüengoitia and DelgadoGranados 2006)

Table 3 Estimated acoustic and seismic energies based on recorded waves

Event number	Acoustic energy ($\times 10^7$ J)	Seismic energy ($\times 10^4$ J)
Event 1	0.6	2.7
Event 2	0.8	4.0
Event 3	9.6	54.3
Event 4	1.4	12.7
Event 5	0.9	11.5

Discussion

Characteristic parameters of the 2015 Aso Strombolian eruptions

Our results show the basic features of the 2015 Aso Strombolian eruptions such as particle sizes, trajectory heights and ejection velocities (Table 1). We also estimated the acoustic energy and seismic energy for each event (Table 3).

Seismic and acoustic waves were recorded by the network of the Aso Volcanological Laboratory of Kyoto University. The acoustic pressure monitored at the ACM station (290 m from the vent, Fig. 1b) was utilized for calculating the acoustic energy. The seismic velocity monitored at the UMA station (830 m from the vent, Fig. 1b) was utilized for calculating the seismic energy. To estimate the explosion energy, we calculated the acoustic and seismic energy using the equations (1) and (2), respectively, from Johnson and Aster (2005). The method of estimating the energies is explained in the Additional file 1 (D).

The values are compared to other Strombolian eruptions (Tables 4, 5). The ejection velocities of large pyroclasts during the 2015 events are 5.1–35.5 m/s, and these are in the range of other Strombolian eruptions, as the 2015 Aso eruptions are the third smallest among the listed eruptions. Sometimes, the ejection velocity of Strombolian eruptions reaches > 100 m/s (Table 4). This comparison simply shows that the size of the 2015 Aso Strombolian eruptions was small in terms of the ejection velocity, but the ejection velocity is in the range of other Strombolian eruptions.

The order of acoustic energy obtained in our study is smaller than the kinetic energy of Gaudin et al. (2014), but larger than other observed eruptions (Table 5). The order of seismic energy was in between the maximum and minimum of other observations (Table 5). Correlation between the acoustic and seismic energies for each event is shown in the Additional file 1 (Fig. S-5).

The relationships between characteristic parameters of events are shown in Fig. 7. The ejection velocity is correlated with the maximum height (Fig. 7a). It is understandably intuitive that a particle released at a faster speed can reach a higher altitude. On the other hand, particle size does not show any correlation with maximum height or ejection velocity (Fig. 7b, c). We often observed that large particles fell on the ground around the vent and the deposited particles decreased in size with distance from the vent. Therefore, we anticipated that there is a negative correlation between the particle size and the kinetic energy at the vent, which can be represented by

Tsunematsu *et al. Earth, Planets and Space*   (2019) 71:49

Page 9 of 14

Table 4 Ballistic ejection velocities of Strombolian eruptions

Eruption	Method of observation	Particle ejection velocity (m/s)	References
Stromboli (Italy)	Doppler radar	7–13	Hort and Seyfried (1998)
Stromboli (Italy)	Photo-ballistics	16–22	Ripepe et al. (1993)
Aso (Japan)	Photo-ballistics	5–35	This Study
Alaid (Kuril, Russia)	Photo-ballistics	6–39	Steinberg and Babenko (1978)
Stromboli (Italy)	Photo-ballistics	35–45	Ripepe et al. (2001)
Erebus (Antarctica)	Doppler radar	7–52	Gerst et al. (2008)
Stromboli (Italy)	Doppler radar	44–70	Hort et al. (2003)
Etna (Italy)	Doppler radar	71	Gouhier and Donnadieu (2010)
Stromboli (Italy)	Photo-ballistics	2–72	Chouet et al. (1974)
Etna (Italy)	Photo-ballistics	15–79	McGetchin et al. (1974)
Stromboli (Italy)	Acoustic sounder	20–80	Weill et al. (1992)
Stromboli (Italy)	Thermal video	3–101	Patrick et al. (2007)
Heimaey (Iceland)	Fall time*	75–110	Self et al. (1974)
Etna (Italy)	Doppler radar	71–119	Gouhier and Donnadieu (2011)
Stromboli (Italy)	Thermal video	9–129	Harris et al. (2012)
Etna (Italy)	Doppler radar	136–163	Dubosclard et al. (2004)
Heimaey (Iceland)	Film tracking	65–230	Blackburn et al. (1976)
Stromboli (Italy)	High-speed imaging	38–405	Taddeucci et al. (2012)

The table is based on Harris et al. (2012), supplemented by data that were published subsequently. This list is sorted with the maximum ejection velocity being in an ascending order from top to bottom. *Fall time method assumes that the drag is minor and thus we can disregard the drag effect

Table 5 Orders of kinetic, acoustic and seismic energies estimated for Strombolian eruptions

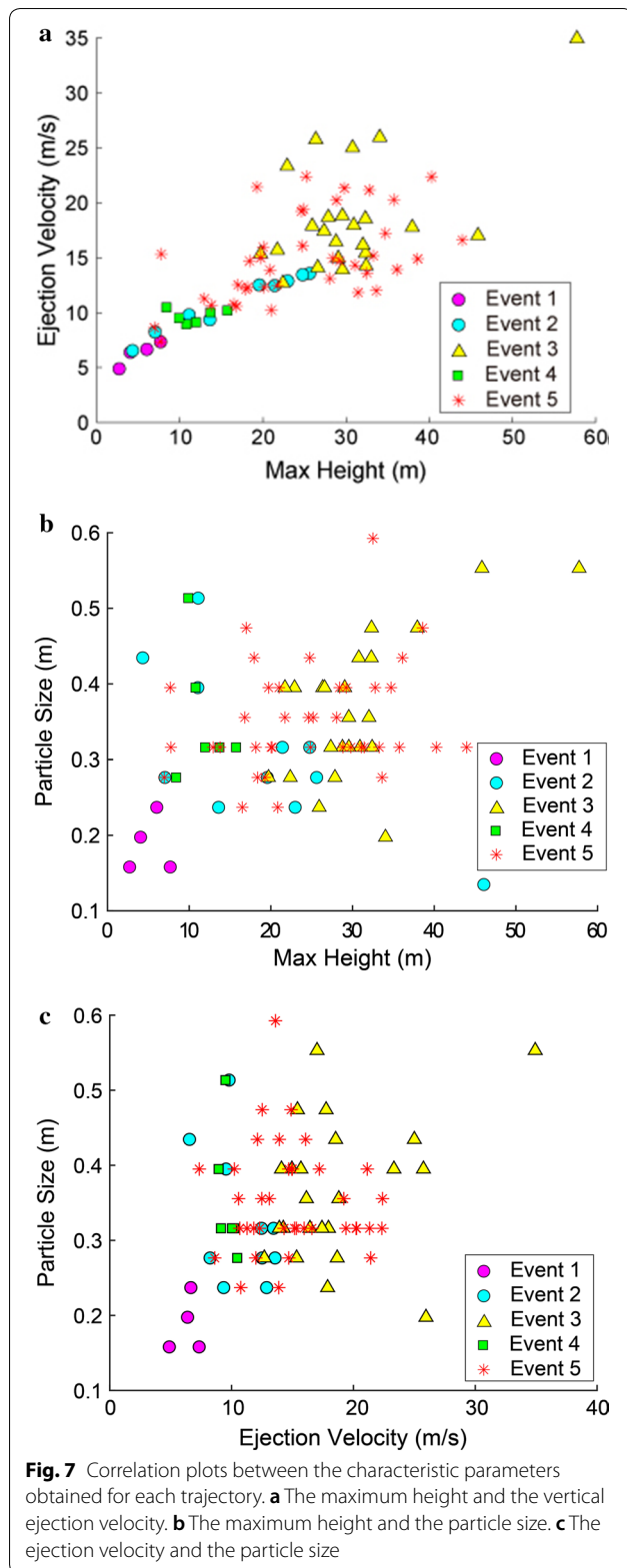| Eruption	Energy type	Energy order of magnitude (J)	References
Stromboli	Kinetic energy	10^3–10^9	Gaudin et al. (2014)
Erebus	Acoustic energy	10^3–10^7	Johnson and Aster (2005)
Karymsky	Acoustic energy	10^3–10^7	Johnson and Aster (2005)
Aso	Acoustic energy	10^6–10^7	This study
Erebus	Seismic energy	10^3–10^7	Johnson and Aster (2005)
Karymsky	Seismic energy	10^3–10^7	Johnson and Aster (2005)
Aso	Seismic energy	10^4–10^5	This study

the maximum height and the ejection velocity. However, as there is no correlation between them, there is no clear relationship between the kinetic energy at the vent and the particle size in observed events.

Explosion and particle release depths

Magma fragmentation is defined as the breakup of a continuous volume of molten rock into discrete pieces, called pyroclasts (Gonnermann 2015). During explosive eruptions, magma is fragmented in the conduit and at a certain depth pyroclasts are thrown into the air. Thus, the explosion depth and the particle release depth are the keys to understanding how pyroclasts are transported.

To obtain the particle release depth, the particle trajectories were extrapolated by straight lines into the conduit (Fig. 8). A similar method was used in Dürig et al. (2015), but we did not use the cut-off angle or the trajectory intersection because the trajectories intersected with each other at multiple points during the same event (Fig. 8). In order to obtain the best fit release depth, we used the convergence point of the trajectories in the blurry image. In other words, the particle release depth was defined as the depth where the width of the bouquet of trajectories was narrowest. The obtained particle release depth and the convergence width are shown in Table 6. The depths were estimated to be within a small range from 11 to 13 m. Trajectory convergence widths in a horizontal direction were within a wider range from 1.4 to 10.6 m.

Ishii et al. (2019) estimated the depth of the explosion to be shallower than 400 m from the vent based on acoustic and seismic data. Observed seismicity is believed to occur as a result of the brittle magma fractures, and the depth obtained by Ishii et al. (2019) is interpreted as the fragmentation depth due to the explosion. Our estimated particle release depths are in the range of their estimation, while the range of the particle release depths based on the trajectories is much shallower than the lower limit value (400 m) of Ishii et al. (2019). The following is a possible scenario if these two types of depths were caused by different reasons; a series of explosions or magma
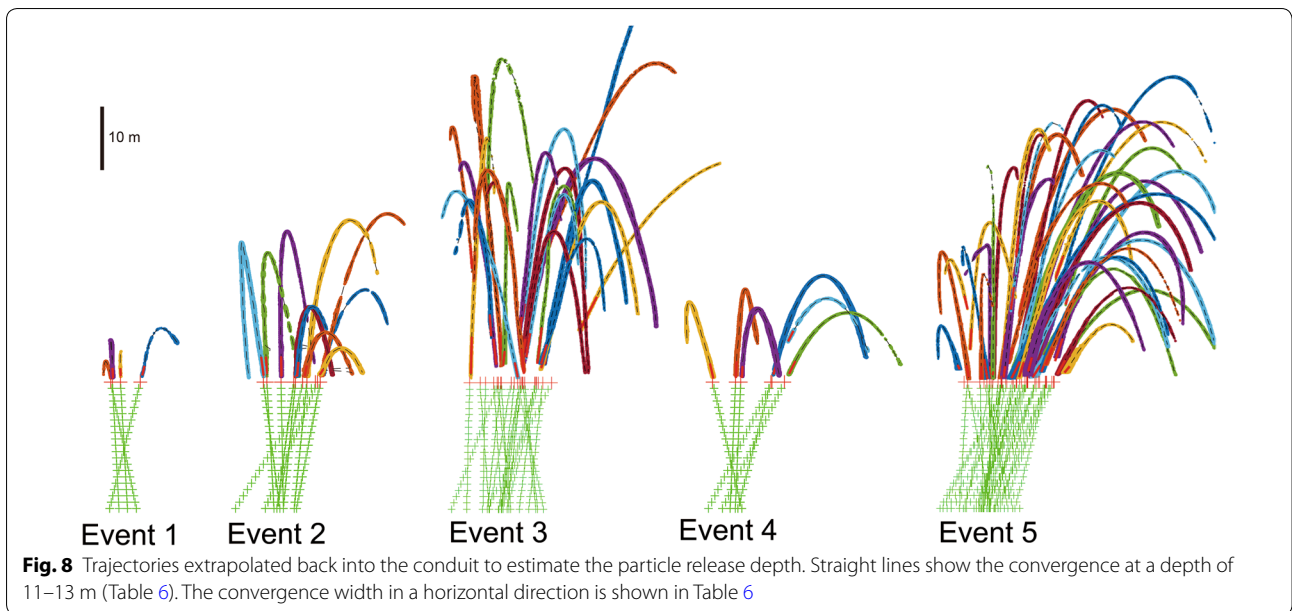
Tsunematsu *et al. Earth, Planets and Space*   (2019) 71:49

Page 10 of 14

Fig. 7 Correlation plots between the characteristic parameters obtained for each trajectory. **a** The maximum height and the vertical ejection velocity. **b** The maximum height and the particle size. **c** The ejection velocity and the particle size

fragmentation probably occurred shallower than 400 m depth, and fragmented magma and gas rose together in the cylindrical conduit. At around the 11–13 m depth, the conduit became wider forming a conical shape and the release of the pressure in the conduit caused the magmatic particles to be thrown into the air.

Probably, the interaction between gas and particles in the conduit affects the particle ejection velocity at the vent. In the future, the relationship between the ejection velocity, the length between fragmentation level and the particle release depth, and the gas flow velocity should be studied experimentally or numerically.

Gas flow and drag effect

The graph in Fig. 6 shows that the estimated gas flow velocity decreases as the assumed drag coefficient increases. This relationship is what we can derive from Eq. (1). According to Eq. (1), the drag term is proportional to the drag coefficient C_D, the squared difference between the particle velocity and the gas flow velocity $(v - u)^2$. If the gas flow velocity is larger than particle velocity $(v < u)$, then the gas flow velocity becomes small when the drag coefficient increases. Our estimation results show that the gas flow velocity is larger than the particle ejection velocity $(v < u)$ and the trend of our estimation is reasonable. However, we cannot estimate the drag coefficient from this process. Taddeucci et al. (2017) estimated the drag coefficient value based on their observation using the high-speed camera. The maximum value of the drag coefficient, calculated using the averaged particle velocity and the flow velocity by Taddeucci et al. (2017), was very large (e.g., $C_D > 3.0$). Their observation only shows a part of the particle trajectories (< 2 s); thus, they could have assumed the velocity was constant only in a small time frame. The particle velocity and the flow velocity, however, vary with time in nature. Therefore, we suspect that the drag coefficient can reach such a high value ($C_D > 3.0$), and it is more realistic to use the drag coefficient values obtained by experiments such as those of Alatorre-Ibargüengoitia and DelgadoGranados (2006) and Bagheri and Bonadonna (2016). The range of drag coefficient measured by Alatorre-Ibargüengoitia and DelgadoGranados (2006) was 0.62–1.01. In this range, the mean gas flow velocity of each event ranges from 25 to 52 m/s. This gas flow velocity range is similar to the value (< 50 m/s) obtained for the Strombolian eruption in the Stromboli volcano by Patrick et al. (2007), based on thermal imagery.

These estimated velocities have a weak correlation with particle size. As shown in Fig. 9, the estimated gas flow velocity increases with particle size. It implies that the larger particles are pushed by the stronger gas flow more than smaller particles when they appear above the vent.

Fig. 8 Trajectories extrapolated back into the conduit to estimate the particle release depth. Straight lines show the convergence at a depth of 11–13 m (Table 6). The convergence width in a horizontal direction is shown in Table 6

Table 6 Estimated particle release depth by linear extrapolation of trajectories

Event number	Particle release depth (m)	Convergence width (m)
Event 1	11	1.4
Event 2	11	5.8
Event 3	12	10.6
Event 4	13	3.0
Event 5	13	10.1

The convergence width of the linear estimation is also shown

Fig. 9 Plots of estimated flow velocity against particle size
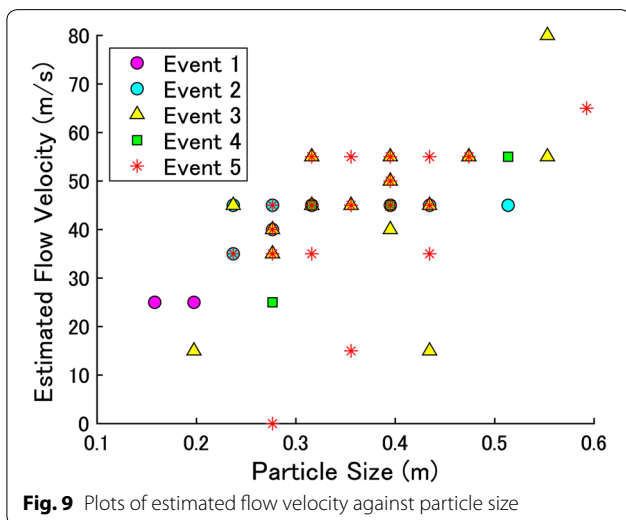
Presumably, the relationship between particle size and the gas flow velocity would be clearer if we had another camera and knew the velocity component away from the camera. Observing the gas flow effect using a three-dimensional view should be tried in the future.

Alatorre-Ibargüengoitia et al. (2011) and Cigala et al. (2017) experimentally showed that the ejection velocity had a negative correlation with the tube length, which was interpreted as the distance from the fragmentation level in the volcanic conduit to the vent surface. Although the mechanism behind the relationship between tube length and ejection velocity is vague, the ascent process of the gas and particle mixture in the conduit controls the ejection velocity and the gas flow velocity after the ejection. As we have shown in the former section, we also obtained the particle release depth. Discussion about the particle and gas transport in the conduit will be possible if we obtain such a dataset from more eruptions.

We could estimate the gas flow velocity based on the comparison between simulated and observed particle trajectories, and these data are possibly useful for governing the transport dynamics of large pyroclasts in Strombolian eruptions, while there is an assumption that the gas flow velocity is constant. However, the gas flow velocity would decrease with time and distance from the vent. In the future, we should directly observe the gas flow and derive the velocity changes; for example, an observation using an infrared camera may enable the visualization of the gas flow velocity. Moreover, if the frame rate and the resolution of video images were higher (e.g., high-speed camera), the observed ejection velocity might be faster and other parameters may be estimated more precisely.

Tsunematsu *et al. Earth, Planets and Space*   (2019) 71:49

Page 12 of 14

The simulation coupled with the gas flow was reported by de' Michieli Vitturi et al. (2017). They implemented the simulation of ballistic projectiles by coupling with the gas flow. They successfully reproduced the deposit distribution of ballistic projectiles from the Mt. Ontake eruption; however, the pressure value was unknown, and they could not clearly discuss how these parameters worked in a real eruption. In this sense, acoustic observation is useful for detecting the pressure change at the time of the eruption. The direct observation with multiple facilities such as high-speed cameras and acoustics could be useful for revealing the gas flow effect.

Conclusions

To mitigate the ballistic hazard, it is necessary to evacuate people from the possible affected area around the vent before an eruption starts. Otherwise, the ballistic projectiles fall on people around the vent because of their fast transport speed. In that sense, we should know the affected area with higher precision. Therefore, we implemented our analysis of large pyroclasts of the 2015 Aso Strombolian eruptions and tried to elucidate the dynamics of the ballistic transport.

We observed the Strombolian events on April 25, 2015, and analyzed the video images for five selected events in order to investigate the gas flow effect on the particle transport of large pyroclasts (> 10 cm). The particle size and the particle number for each event were estimated from cut-out frame images by converting them into binary images. Eighty-two trajectories were obtained by choosing the red-glowing positions, and the maximum height, ejection velocity and ejection angle were estimated from the trajectory data. Moreover, we estimated the particle release depth extrapolating trajectories into the conduit. Finally, the gas flow velocity was estimated varying the drag coefficient C_D by comparing the simulated and observed trajectories.

The ejection velocity of particles ranges from 5.1 to 35.5 m/s. The maximum ejection velocity was the third smallest among the listed Strombolian eruptions.

Depth estimation based on the particle trajectories and the difference of the acoustic–seismic arrival time revealed two depths possibly representing the magma fragmentation depth (< 400 m) and particle release depth (~ 12 m).

The maximum gas flow velocity estimated for each trajectory was 90 m/s, and the velocity values decrease with the drag coefficient. This trend is reasonable based on the theoretical relationship according to Eq. (1), and the range of the gas flow velocity for each event (25–52 m/s) agrees with the estimation of the Strombolian eruption (< 50 m/s) by Patrick et al. (2007). The dataset of the particle release depth and the gas flow velocity are useful for revealing the

particle–gas mixture transport mechanism not only in the air but also in the conduit.

Although we could have estimated the gas flow velocity and investigated aspects of the large pyroclast transport, the dynamics of the transport remain unclear because the gas flow was not observed directly in three dimensions. In the future, it is necessary to observe the large pyroclast transport with the gas flow more carefully at higher resolution and higher frame rate. The numerical model of large pyroclast transport should be improved based on the findings from further observations.

Additional file

Additional file 1. Methods in detail are provided. (A) Defining RGB criteria, (B) Binary Image Analysis, (C) Trajectory Analysis and (D) Acoustic and Seismic energy estimation.

Author details
[1] Faculty of Science, Yamagata University, Yamagata-shi 990-8560, Yamagata, Japan. [2] Mount Fuji Research Institute, Yamanashi Prefectural Government, Japan, 5597-1 Kenmarubi Kamiyoshida, Fujiyoshida-shi 403-0005, Yamanashi, Japan. [3] Department of Geophysics, Graduate School of Science, Kyoto University, Kyoto 606-8502, Kyoto, Japan. [4] Aso Volcanological Laboratory, Graduate School of Science, Kyoto University, Aso-shi 869-2611, Kumamoto, Japan.

Publisher's Note
Springer Nature remains neutral with regard to jurisdictional claims in published maps and institutional affiliations.

References
Alatorre-Ibargüengoitia MA, DelgadoGranados H (2006) Experimental determination of drag coefficient for volcanic materials: calibration and application of a model to Popocatépetl volcano (Mexico) ballistic projectiles. Geophys Res Lett 33:L11302. https://doi.org/10.1029/2006GL026195

Tsunematsu *et al. Earth, Planets and Space*   (2019) 71:49

Page 13 of 14

Alatorre-Ibargüengoitia MA, Scheu B, Dingwell DB, Delgado-Granados H, Taddeucci J (2010) Energy consumption by magmatic fragmentation and pyroclast ejection during Vulcanian eruptions. Earth Planet Sci Lett 291(1–4):60–69. https://doi.org/10.1016/j.epsl.2009.12.051

Alatorre-Ibargüengoitia MA, Scheu B, Dingwell DB (2011) Influence of the fragmentation process on the dynamics of Vulcanian eruptions: an experimental approach. Earth Planet Sci Lett 302(1–2):51–59. https://doi.org/10.1016/j.epsl.2010.11.045

Alatorre-Ibargüengoitia MA, Delgado-Granados H, Dingwell DB (2012) Hazard map for volcanic ballistic impacts at Popocatépetl volcano (Mexico). Bull Volcanol 74(9):2155–2169

Alatorre-Ibargüengoitia MA, Morales-Iglesias H, Ramos-Hernández SG, Jon-Selvas J, Jiménez-Aguilar JM (2016) Hazard zoning for volcanic ballistic impacts at El Chichón Volcano (Mexico). Nat Hazards 81:1733. https://doi.org/10.1007/s11069-016-2152-0

Aster R, MacIntosh W, Kyle P, Esser R, Bartel B, Dunbar N, Johnson J, Karstens R, Kurnik C, McGowan M, McNamara S, Meertens C, Pauly B, Richmond M, Ruiz M (2003) Very long period oscillations of Mount Erebus Volcano, very long period oscillations of Mount Erebus Volcano. J Geophys Res 108(B11):2522. https://doi.org/10.1029/2002JB002101

Bagheri G, Bonadonna C (2016) On the drag of freely falling non-spherical particles. Powder Technol 301:526–544. https://doi.org/10.1016/j.powtec.2016.06.015

Baxter PJ, Gresham A (1997) Deaths and injuries in the eruption of Galeras Volcano, Colombia, 14 January 1993. J Volcanol Geotherm Res 77:325–338

Biass S, Falconec J-L, Bonadonna C, Di Traglia F, Pistolesi M, Rosi M, Lestuzzi P (2016) Great Balls of Fire: a probabilistic approach to quantify the hazard related to ballistics—a case study at La Fossa volcano, Vulcano Island, Italy. J Volcanol Geotherm Res 325:1–14. https://doi.org/10.1016/j.jvolgeores.2016.06.006

Blackburn EA, Wilson L, Sparks RSJ (1976) Mechanisms and dynamics of strombolian activity. J Geol Soc Lond 132:429–440

Bombrun M, Harris A, Gurioli L, Battaglia J, Barra V (2015) Anatomy of a Strombolian eruption: inferences from particle data recorded with thermal video. J Geophys Res Solid Earth 120:2367–2387. https://doi.org/10.1002/2014JB011556

Capponi A, James MR, Lane SJ (2016) Gas slug ascent in a stratified magma: implications of flow organisation and instability for Strombolian eruption dynamics. Earth Planet Sci Lett 435:159–170. https://doi.org/10.1016/j.epsl.2015.12.028

Chouet B, Hamisevicz N, Mcgetchin TR (1974) Photoballistics of volcanic jet activity at Stromboli Italy. J Geophys Res 79:4961–4976

Cigala V, Kueppers U, Peña Fernández JJ, Taddeucci J, Sesterhenn J, Dingwell DB (2017) The dynamics of volcanic jets: temporal evolution of particles exit velocity from shock-tube experiments. J Geophys Res Solid Earth 122:6031–6045. https://doi.org/10.1002/2017JB014149

Cole JW, Cowan HA, Webb TA (2006) The 2006 Raoul Island Eruption—a review of GNS science's actions. GNS Science Report 2006/7 38 p

de' Michieli Vitturi M, Neri A, Esposti Ongaro T, Lo Savio S, Boschi E (2010) Lagrangian modeling of large volcanic particles: application to Vulcanian explosions. J Geophys Res. https://doi.org/10.1029/2009jb007111

de' Michieli Vitturi M, Esposti Ongaro T, Tsunematsu K (2017) Phreatic explosions and ballistic ejecta: a new numerical model and its application to the 2014 Mt. Ontake eruption, IAVCEI 2017 Scientific Assembly Abstract, 246

Dibble RR, Kyle PR, Rowe CA (2008) Video and seismic observations of Strombolian eruptions at Erebus volcano, Antarctica. J Volcanol Geotherm Res 177(3):619–634. https://doi.org/10.1016/j.jvolgeores.2008.07.020

Dubosclard G, Donnadieu F, Allard P, Cordesses R, Hervier C, Coltelli M, Privitera E, Kornprobst J (2004) Doppler radar sounding of volcanic eruption dynamics at Mount Etna. Bull Volcanol 66:443. https://doi.org/10.1007/s00445-003-0324-8

Dürig T, Gudmundsson MT, Dellino P (2015) Reconstruction of the geometry of volcanic vents by trajectory tracking of fast ejecta—the case of the Eyjafjallajökull 2010 eruption (Iceland). Earth Planets Space 67:64. https://doi.org/10.1186/s40623-015-0243-x

Fagents SA, Wilson L (1993) Explosive volcanic eruptions: VII. The ranges of pyroclasts ejected in transient volcanic explosions. Geophys J Int 113:359–370

Fitzgerald RH, Tsunematsu K, Kennedy BM, Breard ECP, Lube G, Wilson TM, Jolly AD, Pawson J, Rosenberg MD, Cronin SJ (2014) The application of a calibrated 3D ballistic trajectory model to ballistic hazard assessments at Upper Te Maari, Tongariro. J Volcanol Geotherm Res 286:248–262. https://doi.org/10.1016/j.jvolgeores.2014.04.006

Gaudin D, Moroni M, Taddeucci J, Scarlato P, Shindler L (2014) Pyroclast Tracking Velocimetry: a particle tracking velocimetry-based tool for the study of Strombolian explosive eruptions. J Geophys Res Solid Earth 119(7):5369–5383. https://doi.org/10.1002/2014JB011095

Gerst A, Hort M, Kyle PR, Vöge M (2008) 4D velocity of Strombolian eruptions and man-made explosions derived from multiple Doppler radar instruments. J Volcanol Geotherm Res 177(3):648–660. https://doi.org/10.1016/j.jvolgeores.2008.05.022

Gonnermann HM (2015) Magma fragmentation. Annu Rev Earth Planet Sci 43:431–458. https://doi.org/10.1146/annurev-earth-060614-105206

Gouhier M, Donnadieu F (2010) The geometry of Strombolian explosions: insights from Doppler radar measurements. Geophys J Int 183(3):1376–1391. https://doi.org/10.1111/j.1365-246X.2010.04829.x

Gouhier M, Donnadieu F (2011) Systematic retrieval of ejecta velocities and gas fluxes at Etna volcano using L-Band Doppler radar. Bull Volcanol 73:1139–1145

Graettinger AH, Valentine GA, Sonder I, Ross PS, White JDL, Taddeucci J (2014) Maar-diatreme geometry and deposits: subsurface blast experiments with variable explosion depth. Geochem Geophys Geosys 15:740–764. https://doi.org/10.1002/2013GC005198

Graettinger AH, Valentine GA, Sonder I, Ross P-S, White JDL (2015) Facies distribution of ejecta in analog tephra rings from experiments with single and multiple subsurface explosions. Bull Volcanol 77:66. https://doi.org/10.1007/s00445-015-0951-x

Harris AJL, Ripepe M, Hughes EA (2012) Detailed analysis of particle launch velocities, size distributions and gas densities during normal explosions at Stromboli. J Volcanol Geotherm Res 231–232:109–131. https://doi.org/10.1016/j.jvolgeores.2012.02.012

Hort M, Seyfried R (1998) Volcanic eruption velocities measured with a micro radar. Geophys Res Lett 25:113–116

Hort M, Seyfried R, Vöge M (2003) Radar Doppler velocimetry of volcanic eruptions: theoretical considerations and quantitative documentation of changes in eruptive behaviour at Stromboli volcano, Italy. Geophys J Int 154:515–532

Houghton BF, Swanson DA, Biass S, Fagents SA, Orr TR (2017) Partitioning of pyroclasts between ballistic transport and a convective plume: Kīlauea volcano, 19 March 2008. J Geophys Res Solid Earth 122:3379–3391. https://doi.org/10.1002/2017JB014040

Iguchi M, Kamo K (1984) On the range of block and lapilli ejected by the volcanic explosions. Disaster Prev Res Inst Annu 27B–1:15–27 **(in Japanese with an English abstract)**

Ishii K, Yokoo A, Kagiyama T, Ohkura T, Yoshikawa S, Inoue H (2019) Gas flow dynamics in the conduit of Strombolian eruptions inferred from seismo-acoustic observations at Aso volcano, Japan. Earth Planets Space 71:13. https://doi.org/10.1186/s40623-019-0992-z

Johnson JB, Aster RC (2005) Relative partitioning of acoustic and seismic energy during Strombolian eruptions. J Volcanol Geotherm Res 148:334–354. https://doi.org/10.1016/j.jvolgeores.2005.05.002

Kilgour G, Manville V, Della Pasqua F, Graettinger A, Hodgson KA, Jolly GE (2010) The 25 September 2007 eruption of Mount Ruapehu, New Zealand: directed ballistics, surtseyan jets, and ice-slurry lahars. J Volcanol Geotherm Res 191:1–14

Mainichi Shimbun (2018) The eruption of Kusatsushirane Volcano, one Self Defense Force Personnel died and 11 people seriously injured, 23 Jan 2018, Mainichi Shimbun, Retrieved from https://mainichi.jp/articles/20180124/k00/00m/040/112000c **(in Japanese)**

Mastin LG (2001) A simple calculator of ballistic trajectories for blocks ejected during volcanic eruptions. U.S. Geological Survey Open-File Report 01-45, 16 pp. Retrieved 1 January, 2016 from http://pubs.usgs.gov/of/2001/0045/

McGetchin TR, Settle M, Chouet BA (1974) Cinder cone growth modeled after Northeast Crater, Mount Etna, Sicily. J Geophys Res 79(23):3257–3272

Meier K, Hort J, Wassermannb M, Garaebiti E (2016) Strombolian surface activity regimes at Yasur volcano, Vanuatu, as observed by Doppler radar, infrared camera and infrasound. J Volcanol Geotherm Res 322:184–195. https://doi.org/10.1016/j.jvolgeores.2015.07.038

Oikawa T, Yoshimoto M, Nakada S, Maeno Komori J, Shimano T, Takeshita Y, Ishizuka Y, Ishimine Y (2016) Reconstruction of the 2014 eruption

Tsunematsu *et al. Earth, Planets and Space*   (2019) 71:49

Page 14 of 14

sequence of Ontake Volcano from recorded images and interviews. Earth Planets Space 68:79. https://doi.org/10.1186/s40623-016-0458-5

Ono K, Watanabe K (1985) Geological map of Aso volcano. Geological Map of Volcanoes, no. 4, Geological Survey of Japan, AIST (**in Japanese with English abstract**)

Patrick MR, Harris AJL, Ripepe M, Dehn J, Rothery DA, Calvari S (2007) Strombolian explosive styles and source conditions: insights from thermal(FLIR) video. Bull Volcanol 69:769–784

Pistolesi M, Delle Donne D, Pioli L, Rosi M, Ripepe M (2011) The 15 March 2007 explosive crisis at Stromboli volcano, Italy: assessing physical parameters through a multidisciplinary approach. J Geophys Res. https://doi.org/10.1029/2011jb008527

Ripepe M, Rossi M, Saccorotti G (1993) Image processing of explosive activity at Stromboli. J Volcanol Geotherm Res 54(3–4):335–351. https://doi.org/10.1016/0377-0273(93)90071-X

Ripepe M, Ciliberto S, Schiava MD (2001) Time constraints for modeling source dynamics of volcanic explosions at Stromboli. J Geophys Res 106(B5):8713–8727

Saito G, Ishizuka O, Ishizuka Y, Hoshizumi H, Miyagi I (2018) Petrological characteristics and volatile content of magma of the 1979, 1989, and 2014 eruptions of Nakadake, Aso volcano, Japan. Earth Planets Space 70:197. https://doi.org/10.1186/s40623-018-0970-x

Self S, Sparks RSJ, Booth B, Walker GPL (1974) The 1973 Heimaey strombolian scoria deposit, Iceland. Geol Mag 111(6):539–548

Shea T, Houghton BF, Gurioli L, Cashman KV, Hammer JE, Hobden BJ (2010) Textural studies of vesicles in volcanic rocks: an integrated methodology. J Volcanol Geotherm Res 190:3–4

Spina L, Taddeucci J, Cannata A, Gresta S, Lodato L, Privitera E, Scarlato P, Gaeta M, Gaudin D, Palladino DM (2015) Explosive volcanic activity at Mt. Yasur: a characterization of the acoustic events (9–12th July 2011). J Volcanol Geotherm Res 322:175–183. https://doi.org/10.1016/j.jvolgeores.2015.07.027

Steinberg GS, Babenko JL (1978) Experimental velocity and density determination of volcanic gases during eruption. J Volcanol Geotherm Res 3:89–98

Stix J, Maarten de Moor J (2018) Understanding and forecasting phreatic eruptions driven by magmatic degassing. Earth Planets Space 70:83. https://doi.org/10.1186/s40623-018-0855-z

Swanson DA, Zolkos SP, Haravitch B (2012) Ballistic blocks around Kīlauea Caldera: their vent locations and number of eruptions in the late 18th century. J Volcanol Geotherm Res 231–232:1–11. https://doi.org/10.1016/j.jvolgeores.2012.04.008

Taddeucci J, Alatorre-Ibargüengoitia MA, Moroni M, Tornetta L, Capponi A, Scarlato AP, Dingwell DB, De Rita D (2012) Physical parameterization

of Strombolian eruptions via experimentally-validated modeling of high-speed observations. Geophys Res Lett 39:L16306. https://doi.org/10.1029/2012gl052772

Taddeucci J, Sesterhenn J, Scarlato P, Stampka K, Del Bello E, Pena Fernandez JJ, Gaudin D (2014) Highspeed imaging, acoustic features, and aeroacoustic computations of jet noise from Strombolian (and Vulcanian) explosions. Geophys Res Lett 41:3096–3102. https://doi.org/10.1002/2014GL059925

Taddeucci J, Alatorre-Ibarguengoitia MA, Palladino DM, Scarlato P, Camaldo C (2015) High-speed imaging of Strombolian eruptions: gas-pyroclast dynamics in initial volcanic jets. Geophys Res Lett 42(15):6253–6260. https://doi.org/10.1002/2015GL064874

Taddeucci J, Alatorre-Ibargüengoitia MA, Cruz-Vázquez O, Del Bello E, Scarlato P, Ricci T (2017) In-flight dynamics of volcanic ballistic projectiles. Rev Geophys 55(3):675–718. https://doi.org/10.1002/2017RG000564

Tsunematsu K, Chopard B, Falcone JL, Bonadonna C (2014) A numerical model of ballistic transport with collisions in a volcanic setting. Comput Geosci 63:62–69. https://doi.org/10.1016/j.cageo.2013.10.016

Tsunematsu K, Ishimine Y, Kaneko T, Yoshimoto M, Fujii T, Yamaoka K (2016) Estimation of ballistic block landing energy during 2014 Mount Ontake eruption. Earth Planets Space 68:88. https://doi.org/10.1186/s40623-016-0463-8

Wardman J, Sword-Daniels V, Stewart C, Wilson T (2012) Impact assessment of the May 2010 eruption of Pacaya volcano, Guatemala. GNS Science Report 2012/09, 90 p

Weill A, Brandeis G, Vergniolle S, Baudin F, Bilbille J, Fevre JF, Piron B, Hill X (1992) Acoustic sounder measurements of the vertical velocity of volcanic jets at Stromboli volcano. Geophys Res Lett 19(23):2357–2360

Yamaoka K, Geshi N, Hashimoto T, Ingebritsen SE, Oikawa T (2016) Special issue "The phreatic eruption of Mt. Ontake volcano in 2014". Earth Planets Space 68:175. https://doi.org/10.1186/s40623-016-0548-4

Yokoo A, Miyabuchi Y (2015) Eruption at the Nakadake 1st Crater of Aso Volcano Started in November 2014. Bull Volcanol Soc Jpn 60(2):275–278 **(in Japanese)**

Yokoo A, Ishii K, Ohkura T, Kim K (2019) Monochromatic infrasound waves observed during the 2014-2015 eruption of Aso volcano, Japan. Earth Planets Space 71:12. https://doi.org/10.1186/s40623-019-0993-y

Zobin VM, Sudo Y (2017) Source properties of Strombolian explosions at Aso volcano, Japan, derived from seismic signals. Phys Earth Planet Inter 268:1–10. https://doi.org/10.1016/j.pepi.2017.05.002